Communication: Transient anion states of phenol…(H2O) n (n = 1, 2) complexes: Search for microsolvation signatures

Eliane M. de Oliveira, Thiago C. Freitas, Kaline Coutinho, Márcio T. do N. Varella, Sylvio Canuto, Marco A. P. Lima, and Márcio H. F. Bettega

Citation: The Journal of Chemical Physics **141**, 051105 (2014); doi: 10.1063/1.4892066

View online: http://dx.doi.org/10.1063/1.4892066

View Table of Contents: http://scitation.aip.org/content/aip/journal/jcp/141/5?ver=pdfcov

Published by the AIP Publishing

Communication: Transient anion states of phenol...$(H_2O)_n$ ($n = 1, 2$) complexes: Search for microsolvation signatures

Eliane M. de Oliveira,[1] Thiago C. Freitas,[2] Kaline Coutinho,[3] Márcio T. do N. Varella,[3] Sylvio Canuto,[3] Marco A. P. Lima,[1] and Márcio H. F. Bettega[4,a)]
[1]*Instituto de Física "Gleb Wataghin", Universidade Estadual de Campinas, 13083-859 Campinas, SP, Brazil*
[2]*Tecnologia em Luteria, Universidade Federal do Paraná, 81520-260 Curitiba, PR, Brazil*
[3]*Instituto de Física, Universidade de São Paulo, CP 66318, 05315-970 São Paulo, SP, Brazil*
[4]*Departamento de Física, Universidade Federal do Paraná, CP 19044, 81531-990 Curitiba, PR, Brazil*

(Received 16 June 2014; accepted 23 July 2014; published online 5 August 2014)

We report on the shape resonance spectra of phenol-water clusters, as obtained from elastic electron scattering calculations. Our results, along with virtual orbital analysis, indicate that the well-known indirect mechanism for hydrogen elimination in the gas phase is significantly impacted on by microsolvation, due to the competition between vibronic couplings on the solute and solvent molecules. This fact suggests how relevant the solvation effects could be for the electron-driven damage of biomolecules and the biomass delignification [E. M. de Oliveira *et al.*, Phys. Rev. A **86**, 020701(R) (2012)]. We also discuss microsolvation signatures in the differential cross sections that could help to identify the solvated complexes and access the composition of gaseous admixtures of these species.
 [http://dx.doi.org/10.1063/1.4892066]

Much of the current knowledge on electron-driven damage to DNA and other biomolecules[1,2] was gained from studies on subunits, such as bases and sugars.[1,3–5] Despite the extensive work on gas-phase collisions, only a few theoretical studies addressed the solvation effects on transient anion states (resonances).[6–9] We recently investigated the role of hydrogen bonding in microsolvated molecules,[8,9] finding out that resonances can be either stabilized or destabilized, depending on the role played by the water molecules in the H-bonds. The π^* resonances located on carbonyl[8] and carboxyl[9] groups were shifted to lower (higher) energies in case the water molecules act as proton donors (acceptors).

While our previous studies addressed target molecules having a single π^* resonance (formaldehyde[8] and formic acid[9]), we presently extend the investigations to phenol. This system is an interesting prototype, sharing a couple of features with the nucleobases: three π^* resonances arising from the six-membered aromatic ring,[10,11] and an indirect dissociative electron attachment (DEA) mechanism involving the second π^* resonance and a σ^*_{OH} anion state.[10,12] It is also the simplest subunit of lignin, a copolymer that could play a central role in the plasma-based treatment of biomass.[10] To investigate the influence of microsolvation on the π^* shape resonances of phenol,[10,11] we consider four complexes, hereafter labeled *A* to *D*, comprising one or two water molecules. The structures are shown in Fig. 1, where the proton donor/acceptor character of the solvent molecules is also indicated. In the following, we report electron scattering calculations to discuss (i) signatures of microsolvation in the differential cross sections (DCS's) that might help to identify the hydrogen-bonded clusters; and (ii) the impact of microsolvation on the π^* shape resonance spectrum and dissociation mechanisms, based on the momentum transfer cross sections (MTCS's) and virtual orbital analysis.

The elastic scattering calculations were performed with the parallel version[13] of the Schwinger multichannel method with pseudopotentials (SMCPP).[14] This variational approach to the scattering amplitude, which relies on a discrete trial set to expand the scattering state, was discussed in detail elsewhere.[13–15] The cross sections were computed in the static-exchange (SE) approximation. While the neglect of correlation-polarization effects in the SE approximation overestimates the resonance energies, some essential aspects of the resonance spectra can be learned from this less computationally expensive approach. The previous studies on microsolvated molecules[8,9] indicated that SE-level cross sections show the same (de)stabilization trends as those obtained in the SE plus polarization (SEP) approximation that accounts for the target dynamical response.

The structures of the complexes (Fig. 1) were obtained from liquid-phase classical Monte Carlo (MC) simulations in the isothermal-isobaric NPT ensemble (P = 1 atm and T = 298 K), as described by Barreto *et al.*[16] The selected phenol...$(H_2O)_n$ clusters are thus representative of H-bonding in the liquid. The intramolecular degrees of freedom were kept frozen during the MC simulations, though the geometries of the complexes and the isolated phenol molecule were subsequently optimized at the second-order Møller-Plesset perturbation (MP2) level employing the aug-cc-pVDZ basis set. The target ground states were then calculated at the Hartree-Fock (HF) level with the basis sets described elsewhere.[10] The canonical HF orbitals were employed to build the SE-approximation scattering states.

Even though the target molecules are polar, the results were not corrected to account for long-ranged dipole potential contribution to the higher partial waves, since the latter only affects the background, having no significant influence

a)Electronic mail: bettega@fisica.ufpr.br

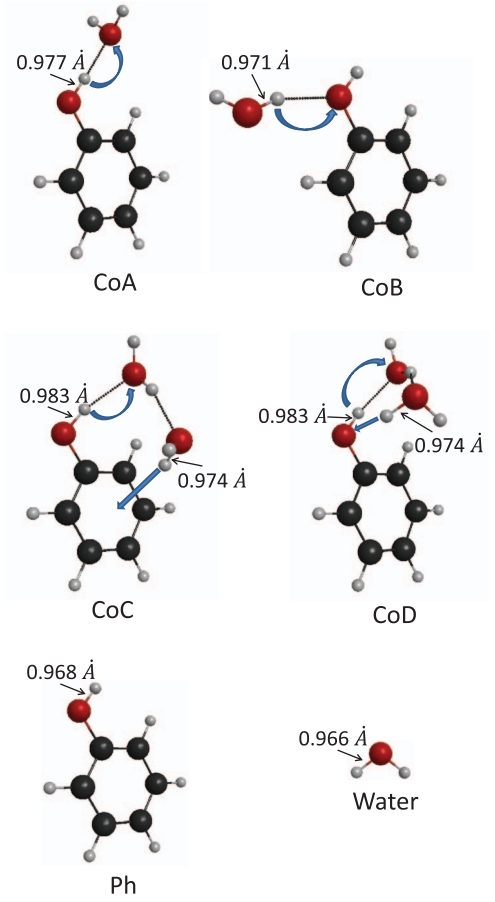

FIG. 1. Structures of the hydrogen-bonded phenol...$(H_2O)_n$ complexes with $n = 1$ (*A* and *B*) and $n = 2$ (*C* and *D*). The isolated phenol (Ph) and water molecules are also shown. The thick arrows are oriented from the proton donors to the acceptors along the H-bonds, while the thin arrows indicate the OH bond lengths. Oxygen, carbon, and hydrogen atoms are shown in red (gray), black, and white, respectively.

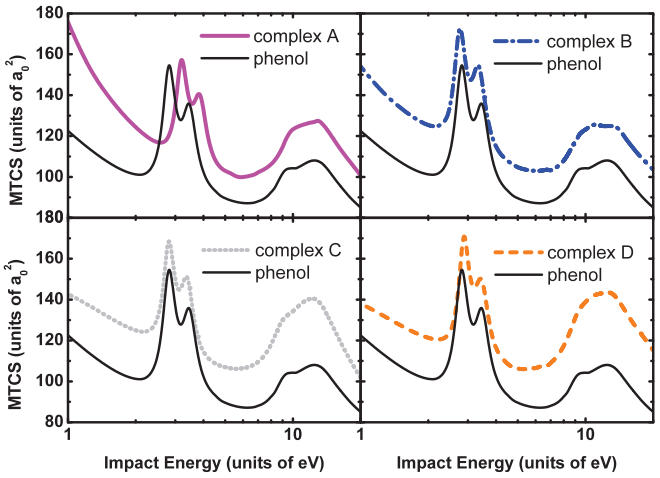

FIG. 2. Momentum transfer cross sections (MTCS), obtained in the SE approximation, for elastic electron scattering by phenol (thin solid line) and the phenol-water complexes shown in Fig. 1.

on the shape resonance spectra. The impact of the dipole correction on the MTCS is also limited by the weighting factor $(1 - \cos\theta)$, where θ is the scattering angle. The calculated dipole moment magnitudes are 4.072 D for complex *A*, 3.199 D for complex *B*, 2.399 D for complex *C*, 1.494 D for complex *D*, and 1.423 D for the isolated phenol molecule. The latter is overestimated with respected to the experimental value of 1.224 D,[17] as usual in HF estimates.

The MTCS's for isolated phenol and the four complexes are shown in Fig. 2, where the signatures of the three π^* resonances are clear in all cases. The energies (E_{res}) and widths (Γ) of the lowest-lying anion states, π_1^* and π_2^*, as obtained from least-squares fits to the eigenphase sums,[18] are shown in Table I. Although the SE approximation overestimates the positions of the three resonances, we did not consider the highest π_3^* anion state (broader peak around 10 eV), as it would have a mixed shape and core-excited character,[19–21] such that larger errors would be expected for the location of this resonance. The SE approximation is thus inadequate as the lack of configurations built on excited target states hinder both the description of polarization effects (as in the π_1^* and π_2^* resonances) and the mixed character. The inspection of the resonance positions (Table I) suggests that microsolvation shifts the resonance positions to higher (lower) energies for the complex *A* (*B*), in consistency with the previous studies,[8,9] which pointed out resonance upshifts (downshifts) in complexes wherein the water molecules H-bonded to the solute act as proton acceptors (donors). No significant shifts or clear trends are found for the complexes *C* and *D*, comprising two water molecules. In these systems, the solute molecules would in principle become more negatively charged as they act as proton donors in the H-bonds. However, the additional water molecules seem to counterbalance the charge transfer, as the protons interact with the hydroxyl group (*D*) or the ring (*C*), resulting in no significant (de)stabilization of the resonances.

Figure 3 shows the lowest unoccupied virtual orbitals (LUMO's) of phenol and the complexes *A* and *B*, as obtained from the compact 6-31G(*d*) basis set built into GAMESS,[23] which are routinely employed to support electron transmission spectroscopy (ETS) assignments.[22] In all cases, the LUMO and LUMO+1 have π^* characters and can be associated with the π_1^* and π_2^* resonances, while the LUMO+2 has a σ_{OH}^* character, either located in the hydroxyl groups of phenol (complex *B*) or solvent molecules (complexes *A*, *C*, and *D*); the LUMO plots for the complexes *C* and *D* are shown in the supplementary material.[18] This fact, along with the DEA data for phenol,[12] is consistent with the existence of σ_{OH}^* resonances, even though these are not evident in the MTCS's. As discussed elsewhere,[5,10,13,24–26] the σ_{NH}^* and σ_{OH}^*

TABLE I. π^* resonance positions (E_{res}) and widths (Γ), in units of eV, for phenol and the phenol...$(H_2O)_n$ complexes, with $n = 1$, 2, shown in Fig. 1. The resonance parameters were obtained from fits to the SE-level eigenphase sums.[18]

System	$E_{res}(\pi_1^*)$	$\Gamma(\pi_1^*)$	$E_{res}(\pi_2^*)$	$\Gamma(\pi_2^*)$
Phenol	2.81	0.47	3.43	0.60
Complex *A*	3.20	0.51	3.83	0.64
Complex *B*	2.74	0.41	3.30	0.60
Complex *C*	2.81	0.38	3.35	0.58
Complex *D*	2.82	0.47	3.41	0.64

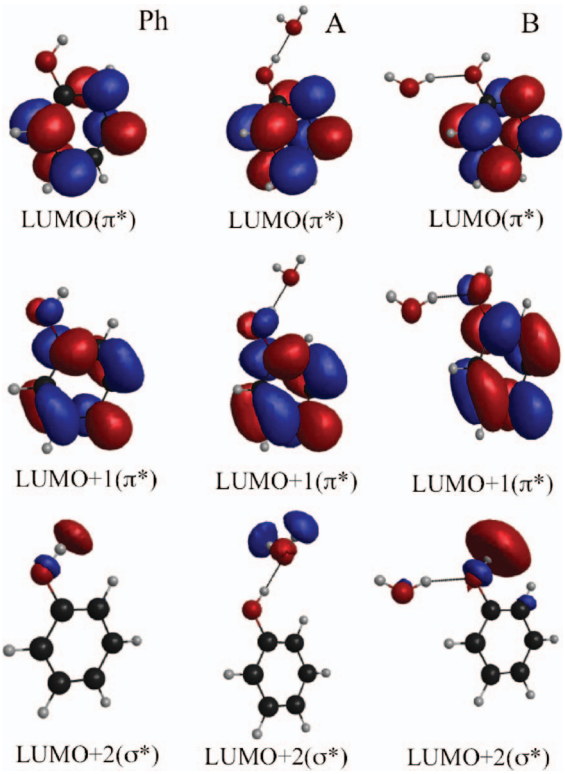

FIG. 3. Lowest-lying virtual orbitals obtained with compact basis sets for phenol (left column), complex *A* (center), and complex *B* (left). The π^* and σ^* characters are indicated in the panels. The plots were generated with MacMolPlt.[31]

anion states in biomolecules are usually broad (coupled to the barrierless *s* wave), embedded into a very large background arising from the dipole interaction, and often diabatically coupled to dipole-supported bound states. Their signatures in the elastic scattering data are usually unclear, if not absent, although their existence is supported by DEA and electron energy loss experiments (see, for instance, Refs. 25 and 26). As previously pointed out,[10] the virtual orbital (VO) analysis for isolated phenol also indicates that electron attachment to the π_2^* anion should lead to hydrogen elimination from the hydroxyl group, as the LUMO+1 and LUMO+2 densities around the oxygen atom favor the π_2^*/σ_{OH}^* vibronic coupling (similar analysis are consistent with the DEA data for a number of biomolecules having aromatic rings, e.g., pyrrole,[5,27] nucleobases,[28] and halouracils[24,29]). However, in the microsolvated complexes *A*, *C*, and *D*, the σ_{OH}^* VO's are located on solvent molecules; only in the complex *B*, where the donor character enhances the negative charge on the water molecule, this orbital remains localized in the solute. These facts strongly indicate that the vibronic coupling could be shifted to the solvent, suppressing the H elimination from phenol. The H–OH dissociation of solvent molecules would also be expected, though the DEA threshold (3.27 eV in isolated water molecules[30]) could prevent this process in small clusters.

Electron interactions with microsolvated molecules would be expected to pose a number of challenges to experimentalists, such that pointing out signatures of clusterization is an essential point. To address the microsolvation signatures

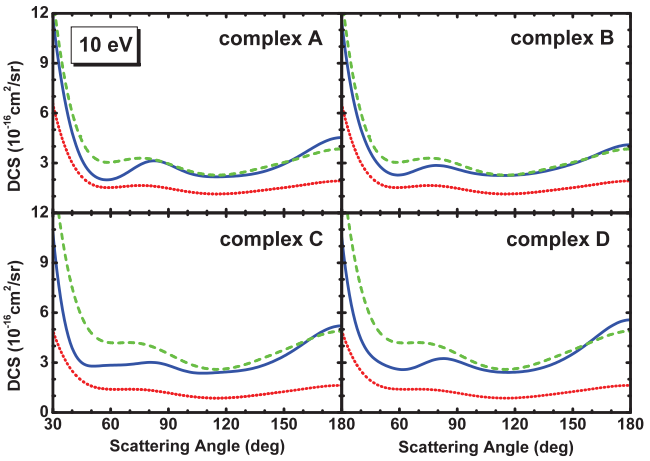

FIG. 4. Differential cross sections (DCSs) at 10 eV for elastic electron scattering by the phenol-water complexes shown in Fig. 1 (solid lines), obtained in the SE approximation. The dashed lines are the DCSs for the molecular "groups" described in the text (DCS^{grp}). The dotted lines are the DCSs for gaseous admixtures (DCS^{adm}).

in the DCS, we consider electron scattering in three scenarios. (i) A gas of phenol-water complexes comprising the same number of water molecules (n_w), i.e., with the same $1{:}n_w$ (solute:solvent) ratio. (ii) A cluster-free gaseous admixture of phenol and water, with the phenol concentration also given by $1{:}n_w$, i.e., the admixture that would be obtained if all the intermolecular bonds in (i) were broken. (iii) A fictitious gas where the electrons would be incoherently scattered by "groups" with the same $1{:}n_w$ ratio. The cross sections would be affected by the group size, although no interference between scattering from different molecules within the group would take place. In the case (ii), the DCS is given by the concentration average over the components, $DCS^{adm} = 1/(1+n_w)DCS^{phenol} + n_w/(1+n_w)DCS^{water}$, while in the case (iii) it is given by the weighted sum $DCS^{grp} = DCS^{phenol} + n_w DCS^{water}$. Comparing DCS^{adm} and DCS^{grp} thus points out size effects (arising from the groups of molecules), while the comparison between the latter and the complex cross section (DCS^{cmp}) would highlight interference effects. Since DCS measurements are intrinsically averaged over the target orientations, the differences between DCS^{grp} and DCS^{cmp} also arise from averaging over the complex orientations (the molecules rotate together, ideally as a rigid body) and over the orientations of individual molecules in the group (the molecules rotate independently).

The DCS results at 10 eV are shown in Fig. 4 for scattering angles ($\theta \geq 30^o$) not significantly affected by the dipole potential (see the supplementary material[18] for other energies). We present calculations for the *A*–*D* complexes (DCS^{cmp}), along with the predictions for the phenol-water admixtures (DCS^{adm}) and the fictitious gas (DCS^{grp}), as obtained from the DCS's of the isolated species. In general, the DCS^{adm} magnitudes are significantly smaller than those of DCS^{cmp} and DCS^{grp}, thus suggesting the size effects could be helpful to distinguish clusters with different numbers of water molecules. While interference and orientation averages give rise to discrepancies between DCS^{cmp} and DCS^{grp} at lower scattering angles ($\lesssim 80^o$), both results are often very similar above $\theta \gtrsim 100^o$. At least for small clusters, this finding

could provide valuable guidance to identify the microsolvated species: the DCS measurements are fairly precise, with errors below 20%, and the DCS^{grp} estimates can be easily obtained from the DCS's of the isolated solute and solvent molecules. Although we dot not further explore the microsolvation signatures, DCS estimates for more realistic gases, i.e., admixtures of complexes comprising different numbers of water molecules, could be easily obtained from concentration averages of the appropriate DCS^{grp} predictions. We also mention that the optimized clusters addressed in this work would reflect those present in supersonic jet expansions, also pointing out the donor/acceptor role of the water molecules in H bonds and their influence in the experimental data.[16,32]

In summary, the SE-level calculated cross sections indicate the expected (de)stabilization trends for the H-bonded phenol-water clusters. These results, along with the VO analysis, also point out that microsolvation impacts the π_2^*/σ_{OH}^* dissociation mechanism observed in the gas phase, possibly switching off the hydrogen elimination from the solute. This fact suggests how significantly the solvation effects could impact the physical chemical basis for electron-driven damage to biomolecules and the biomass delignification. The DCS results also point out microsolvation signatures that could help to access the composition of gaseous admixtures of microsolvated molecules.

The authors acknowledge support from the Brazilian agencies FAPESP and CNPq. This work was supported by the CNPq/NSF Cooperative Research Program and by the FAPESP Bioenergy Program (BIOEN 08/58034-0). The present calculations were performed at CENAPAD/SP, CTBE/CNPEM, IFGW/UNICAMP, LFTC-DFis-UFPR, and LCPAD-UFPR. M.H.F.B. acknowledges computational support from Professor C. de Carvalho.

[1]For a review, see L. Sanche, Eur. Phys. J. D **35**, 367 (2005).
[2]C.-R. Wang, J. Nguyen, and Q.-B. Lu, J. Am. Chem. Soc. **131**, 11320 (2009).
[3]I. Baccarelli, I. Bald, F. A. Gianturco, E. Illenberger, and J. Kopyra, Phys. Rep. **508**, 1 (2011).
[4]M. H. F. Bettega and M. A. P. Lima, J. Chem. Phys. **126**, 194317 (2007).
[5]E. M. de Oliveira, M. A. P. Lima, M. H. F. Bettega, S. d'A. Sanchez, R. F. da Costa, and M. T. do N. Varella, J. Chem. Phys. **132**, 204301 (2010).
[6]I. Baccarelli, A. Grandi, F. A. Gianturco, R. R. Lucchese, and N. Sanna, J. Phys. Chem. B **110**, 26240 (2006).
[7]I. I. Fabrikant, S. Caprasecca, G. A. Gallup, and J. D. Gorfinkiel, J. Chem. Phys. **136**, 184301 (2012).
[8]T. C. Freitas, M. A. P. Lima, S. Canuto, and M. H. F. Bettega, Phys. Rev. A **80**, 062710 (2009).
[9]T. C. Freitas, K. Coutinho, M. T. do N. Varella, M. A. P. Lima, S. Canuto, and M. H. F. Bettega, J. Chem. Phys. **138**, 174307 (2013).
[10]E. M. de Oliveira, S. d'A. Sanchez, M. H. F. Bettega, A. P. P. Natalense, M. A. P. Lima, and M. T. do N. Varella, Phys. Rev. A **86**, 020701(R) (2012).
[11]K. D. Jordan, J. A. Michejda, and P. D. Burrow, J. Am. Chem. Soc. **98**, 7189 (1976).
[12]R. V. Khatymov, M. V. Muftakhov, and V. A. Mazunov, Rapid Commun. Mass Spectrom. **17**, 2327 (2003).
[13]J. S. dos Santos, R. F. da Costa, and M. T. do N. Varella, J. Chem. Phys. **136**, 084307 (2012).
[14]M. H. F. Bettega, L. G. Ferreira, and M. A. P. Lima, Phys. Rev. A **47**, 1111 (1993); R. F. da Costa, F. J. da Paixão, and M. A. P. Lima, J. Phys. B **37**, L129 (2004).
[15]K. Takatsuka and V. McKoy, Phys. Rev. A **24**, 2473 (1981); **30**, 1734 (1984).
[16]R. C. Barreto, K. Coutinho, H. C. Georg, and S. Canuto, Phys. Chem. Chem. Phys. **11**, 1388 (2009).
[17]*CRC Handbook of Chemistry and Physics*, 79th ed., edited by D. R. Lide (CRC, Boca Raton, 1998).
[18]See supplementary material at http://dx.doi.org/10.1063/1.4892066 for the notes on the fitting of the eigenphase sum and virtual orbital plots not shown here.
[19]I. Nenner and G. J. Schulz, J. Chem. Phys. **62**, 1747 (1975).
[20]C. Winstead and V. McKoy, Phys. Rev. Lett. **98**, 113201 (2007); Phys. Rev. A **76**, 012712 (2007).
[21]Z. Mažín and J. D. Gorfinkiel, J. Chem. Phys. **135**, 144308 (2011).
[22]A. Modelli and P. W. Burrow, J. Phys. Chem. A **108**, 5721 (2004).
[23]M. W. Schmidt, K. K. Baldridge, J. A. Boatz, S. T. Elbert, M. S. Gordon, J. H. Jensen, S. Koseki, N. Matsunaga, K. A. Nguyen, S. J. Su, T. L. Windus, M. Dupuis, and J. A. Montgomery, J. Comput. Chem. **14**, 1347 (1993).
[24]F. Kossoski, M. H. F. Bettega, and M. T. do N. Varella, J. Chem. Phys. **140**, 024317 (2014).
[25]G. Gallup, P. Burrow, and I. Fabrikant, Phys. Rev. A **79**, 042701 (2009); **80**, 046702 (2009).
[26]A. M. Scheer, P. Mozejko, G. A. Gallup, and P. D. Burrow, J. Chem. Phys. **126**, 174301 (2007).
[27]K. R. Asmis and M. Allan, Pyrrole data in the *Gallery of unpublished EEL spectra*, see http://www.chem.unifr.ch/ma/dir_allan/pyrrole_EELS.pdf.
[28]D. Burrow, G. A. Gallup, A. M. Scheer, S. Denifl, S. Ptasinska, T. Märk, and P. Scheier, J. Chem. Phys. **124**, 124310 (2006).
[29]S. Denifl, S. Ptasinska, G. Hanel, B. Gstir, M. Probst, P. Scheier, and T. D. Märk, J. Chem. Phys. **120**, 6557 (2004).
[30]D. J. Haxton, C. W. McCurdy, and T. N. Rescigno, Phys. Rev. A **75**, 012710 (2007).
[31]B. M. Bode and M. S. Gordon, J. Mol. Graphics Modell. **16**, 133 (1998).
[32]K. Fuke and K. Kaya, Chem. Phys. Lett. **94**, 97 (1983).